ORGANOMETALLICS

Article

pubs.acs.org/Organometallics

Catalytic Intramolecular Hydroamination with a Bifunctional Iridium Pyrazolato Complex: Substrate Scope and Mechanistic Elucidation

Yohei Kashiwame, Shigeki Kuwata,* and Takao Ikariya*

Department of Applied Chemistry, Graduate School of Science and Engineering, Tokyo Institute of Technology, O-okayama, Meguro-ku, Tokyo 152-8552, Japan

Supporting Information

ABSTRACT: Catalytic intramolecular cyclization of nonactivated aminoalkene with functional group compatibility provides an atom-economical and concise route to valuable nitrogen-containing heterocycles yet remains a challenge. In this paper, we report the detailed substrate scope and mechanism of catalytic intramolecular hydroamination with a half-sandwich-type iridium pyrazolato complex we have recently developed. This metal−ligand bifunctional catalyst promoted the hydroamination of various primary and secondary aminoalkenes at mild temperatures (50−110 °C) without side reactions such as oxidative amination. Cyclization of secondary aminoalkenes containing ester, cyano, bromo, and hydroxy groups occurred with maintenance of these functional groups, while the reactions of aminoalkenes bearing allylic substituents proceeded with a perfect diastereoselectivity. Catalyst optimization revealed that the proton-responsive functional group at the position β to the metal is crucial to efficient catalytic turnover. Kinetic analysis indicated a highly ordered transition state associated with N−H bond cleavage in the rate-determining step. On the basis of these data along with the stoichiometric reactions and DFT calculations, we propose an unprecedented metal−ligand cooperating mechanism, in which cyclization occurs through *syn* addition of the amino group to the coordinated olefin bond with the aid of the Brønsted basic pyrazolato ligand.

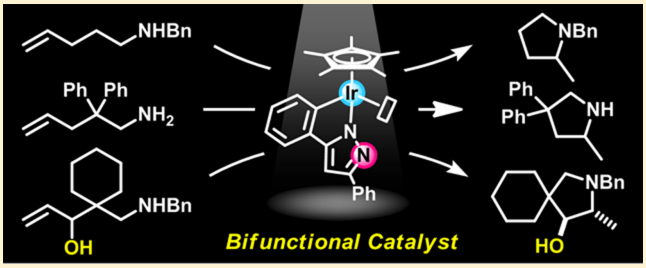

INTRODUCTION

Intramolecular hydroamination of aminoalkenes is a powerful, straightforward, and atom-economical methodology to access cyclic amines, which are useful building blocks for a vast number of bioactive natural alkaloids and other pharmaceutical compounds. Intensive efforts have thus been devoted to the development of efficient and practical hydroamination catalysts.[1] Currently the most active catalysts for the cyclization of simple aminoalkenes, in which the olefin bond is not activated by conjugation or electron-withdrawing substituents, contain group 2−4 metals as a key component.[2,3] These catalysts are, however, scarcely compatible with polar functional groups as well as air and moisture due to the highly Lewis acidic nature of the metals. Late-transition-metal catalysts are more promising in this regard, and actually, those with increased substrate scope and functional group tolerance have been reported during the past decade.[4−11] Rational improvement of the late-metal catalysts is still required in order to promote the cyclization of relatively inert aminoalkenes, such as those with a less nucleophilic primary amino group and those lacking *gem* substituents on the chain that facilitate the cyclization by a Thorpe−Ingold effect,[12] under mild conditions. Judicious catalyst design is also crucial to control the stereochemistry of the cyclization product, which has rarely been explored in late-metal catalysis,[13] and to avoid undesired side reactions exemplified by the formation of imines and olefin isomerization.

The reaction mechanisms of hydroamination of nonactivated olefins with late-transition-metal catalysts are roughly divided into two categories.[1] One involves primary N−H bond cleavage followed by alkene insertion into the resulting metal−amido bond, and the other entails nucleophilic attack of the amine at the π-coordinated olefin. In each case, either the amino or the olefin group undergoes primary activation. We considered that simultaneous activation of both functional groups by the metal−ligand bifunctional catalysts, in which the Brønsted acidic and basic ligands take part in the catalysis through hydrogen bonding and proton transfer,[14−16] would lead to the development of novel hydroamination catalysts for a broader range of substrates with higher efficiency.

As an extension of our continuing study of metal−ligand bifunctional catalysis,[14,15] we recently communicated that the protic pyrazole complex **1** as well as its dehydrochlorinated form **2** catalyzes cyclization of both primary and secondary aminoalkenes at a fairly low temperature (50 °C), as shown in eq 1.[17] Importantly, a preliminary catalyst survey revealed that the proton-responsive functional group placed at the position β to the metal is crucial to the catalysis, suggesting that a bifunctional mechanism based on the metal−ligand cooperation is operative. We report here the broad substrate scope and remarkable selectivity of this novel bifunctional pyrazole

Received: November 7, 2012
Published: November 19, 2012

dx.doi.org/10.1021/om301063n | *Organometallics* 2012, 31, 8444−8455

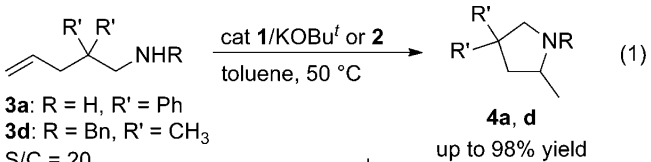

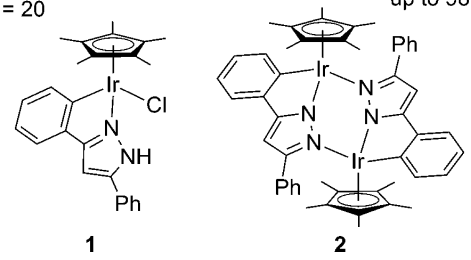

catalyst as well as the mechanistic details elucidated by stoichiometric reactions, kinetic experiments, and theoretical calculations.

RESULTS AND DISCUSSION

Catalyst Screening and Solvent Dependence. To corroborate the importance of the β-NH group in the bifunctional pyrazole catalyst **1**, we initially prepared a series of related C−N chelate half-sandwich-type iridium complexes **5**−**7** and assessed the catalytic activity toward intramolecular hydroamination of the ω-alkenic primary amine **3a**. Masking of the NH group in **1** was achieved by the reaction of the pyrazolato-bridged dimer **2** with iodomethane, giving the *N*-methylpyrazole complex **5** (eq 2). We additionally synthesized

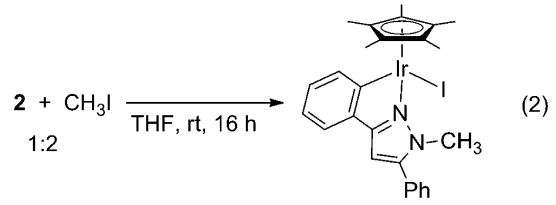

the C−N chelate imidazole complex **6**, wherein the NH group lies at the position γ to the metal,[17,18] by acetate-promoted cyclometalation of 2-phenylimidazole. These modified azole complexes **5** and **6** exhibited only poor catalytic activity (Table 1, entries 6 and 7), unlike the β-protic complex **1** (entry 1). On the other hand, the pyrazolato-bridged dimer **2** was almost as efficient as the **1**/KOBu^t binary catalyst even in the absence of the base (entry 1 vs 4), indicating that the dehydrochlorinated mononuclear bifunctional species is the catalytically active intermediate. In contrast, the amido complex **7**[19] obtained by dehydrochlorination of an α-protic amine chlorido complex was totally ineffective toward intramolecular hydroamination (entry 8). These observations imply that the proton-responsive group built in a suitable position of the ligand is involved directly in the catalysis.

A wide range of solvents can be employed in this catalytic hydroamination. The high efficiency of the pyrazolato-bridged dimer **2** was preserved in the coordinating solvents THF and acetonitrile, as shown in entries 10 and 11, which promises catalyst compatibility with Lewis basic functional groups in the substrates. The reaction in methanol was much slower (entry 12), probably due to concomitant transfer hydrogenation of the pyrazolato complex with the alcohol.[17] Julian and Hartwig[5] demonstrated that cyclization of aminoalkenes with a catalyst

Table 1. Intramolecular Hydroamination Catalyzed by C−N Chelate Complexes[a]

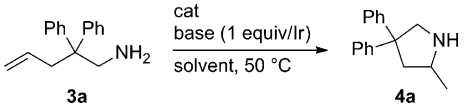

entry	cat.	base	solvent	*t*, h	yield,[b] %
1	**1**	KOBu^t	toluene	6	75
2	**1**	KOBu^t	toluene	15	98
3	**1**	none	toluene	6	29
4	**2**	none	toluene	6	80
5	**2**	none	toluene	15	96
6	**5**	KOBu^t	toluene	6	8
7	**6**	KOBu^t	toluene	15	20
8	7	none	toluene	15	0
9	none	KOBu^t	toluene	6	0
10	**2**	none	THF	6	84
11	**2**	none	acetonitrile	6	73
12	**2**	none	methanol	6	17
13	**2**	none	*tert*-butyl alcohol	6	5
14	**2**	none	$ClCH_2CH_2Cl$	6	0

[a]Conditions: **3a**:Ir = 20:1, [**3a**] = 0.2 M. [b]Determined by ^{1}H NMR analyses.

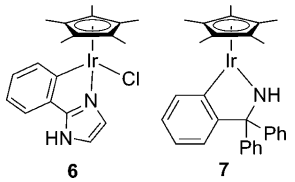

composed of $[Rh(cod)(CH_3CN)_2]BF_4$ and a bis(diethylamino) derivative of xantphos proceeds in *tert*-butyl alcohol with high efficiency and selectivity, which may be ascribed to facile proton transfer in the turnover-limiting step; however, this solvent proved less effective in our catalyst system (entry 13), possibly because of the low catalyst solubility. No cyclization product was obtained from the reaction in 1,2-dichloroethane under otherwise identical reaction conditions (entry 14).

Substrate Scope and Limitations. The scope of the substrates for intramolecular hydroamination catalyzed by the pyrazolato-bridged dimer **2** is summarized in Table 2. Cyclization of the primary aminoalkene **3b** with a sterically crowded 1,1-disubstituted olefin bond was completed at a higher temperature (entry 2) in comparison to the case for the less substituted congener **3a** (entry 1). The reactions of the more nucleophilic secondary amines **3c**−**f** were readily accomplished with much lower catalyst loadings (1 mol %; entries 3−6). It should be noted that side products due to β-hydride elimination were not observed at all in these hydroamination reactions. Notably, the allyl-branched aminoalkene **3f** yielded the cyclization product with a perfect trans/cis diastereoselectivity (entry 6). The stereochemistry was determined by an X-ray analysis of the HBF_4 salt of the product (Figure 1). Such successful control of the relative configuration of two adjacent stereogenic centers through intramolecular hydroamination is very rare.[20] It is also remarkable that the *N*-benzylaminoalkene **3g**, unbiased toward cyclization by the chain substituents, was converted to the hydroamination product in excellent yield at 80 °C (entry 7). Indeed, hydroamination of this class of substrates is rarely achieved by late-transition-metal catalysts.[5−7] Formation of a six-

dx.doi.org/10.1021/om301063n | *Organometallics* 2012, 31, 8444−8455

Table 2. Substrate Scope of the Hydroamination Catalyzed by 2[a]

entry	aminoalkene	product	S/C[b]	temp., °C	yield, %[c]
1	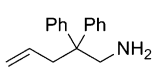 **3a**	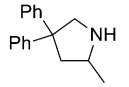 **4a**	20	50	89
2	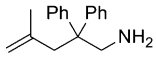 **3b**	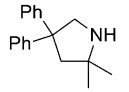 **4b**	20	110	91
3	 **3c**	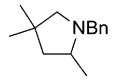 **4c**	100	50	66
4	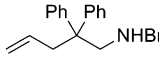 **3d**	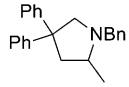 **4d**	100	50	>99
5	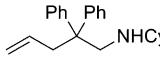 **3e**	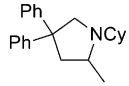 **4e**	100	50	93
6	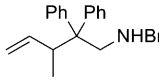 **3f**	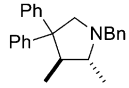 **4f**	100	50	99 (>95:5 *dr*[d])
7	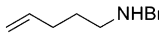 **3g**	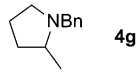 **4g**	20	80	98
8	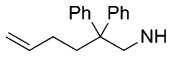 **3h**	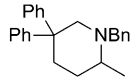 **4h**	20	110	70
9	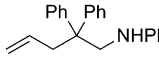 **3i**	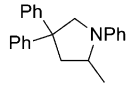 **4i**	20	110	61[e]
10	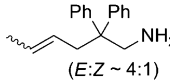 **3j** (*E*:*Z* ~ 4:1)	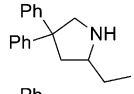 **4j**	20	50	0
11	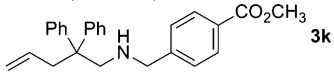 **3k**	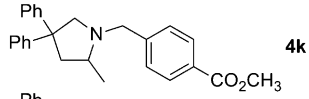 **4k**	100	50	94
12	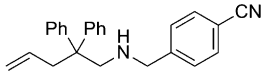 **3l**	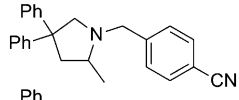 **4l**	100	50	96
13	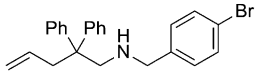 **3m**	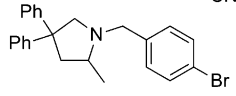 **4m**	100	50	97
14	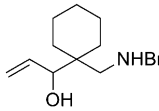 **3n**	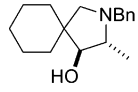 **4n**	100	50	86 (>95:5 *dr*[d])

[a]Reaction conditions: **3** (0.2 M in toluene), **2**, 15 h. [b]Ratio of **3** to iridium. [c]Isolated yield. [d]Determined by ^{1}H NMR analyses. [e]Determined by ^{1}H NMR analysis using durene as an internal standard.

membered ring (entry 8) as well as cyclization of an arylamine **3i** (entry 9) proved to be sluggish and required higher temperatures. In contrast, hydroamination of an internal alkene **3j** did not proceed at all (entry 10).

The bifunctional pyrazolato catalyst **2** was found to exhibit wide functional group compatibility. Substrates bearing ester or cyano groups underwent hydroamination with maintenance of these functional groups to afford the corresponding cyclic amines quantitatively (entries 11 and 12). An aryl bromide moiety also remains intact (entry 13), implying that the catalysis does not involve low-valent coordinatively unsaturated intermediates that would suffer oxidative addition of the C−Br bond. To our knowledge, hydroamination catalysts compatible with the aryl bromide function are limited to only two catalyst systems.[8] Strikingly, cyclization of the substrate **3n** bearing a secondary hydroxy group at the allylic position took place to give the desired cyclic amine as a single diastereomer (entry 14), despite the fact that the catalyst **2** oxidizes 2-propanol[17] and the catalysis is retarded in alcohols (vide supra). Only a small amount of saturated ketones derived from substrate isomerization and product oxidation were produced concomitantly in variable yields (8% and 3% at most, respectively). Oxidation of the hydroxy group may be suppressed by steric hindrance of the substrate **3n**. The *anti* configuration of **4n**, similar to that of **4f** (entry 6), was confirmed by 1D NOE difference ^{1}H NMR experiments, as summarized in Chart 1. An NOE correlation between the methyl protons and the neighboring vicinal methine proton was observed, while an interaction between the two vicinal methine protons was not detected (see the Supporting Information). Liu and Hartwig[6]

dx.doi.org/10.1021/om301063n | *Organometallics* 2012, 31, 8444−8455

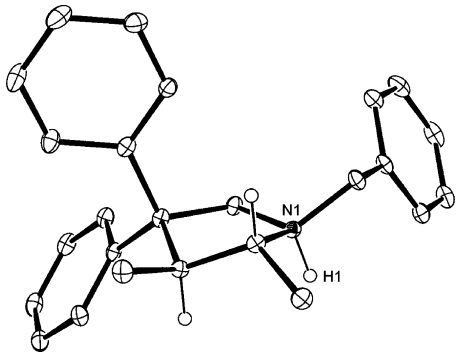

Figure 1. Structure of **4f**·HBF_4. One of the two crystallographically independent molecules is shown. The anion and hydrogen atoms, except for the NH proton and the methine protons, are omitted for clarity.

Chart 1. The NOE Correlation in 4n

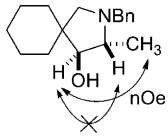

reported that intramolecular hydroamination of **3n** with a rhodium−biarylphosphine catalyst affords the cyclization product with an 11:1 diastereomer ratio. The major product in their reaction is not identical with **4n** in the ^{1}H NMR criteria,[21] suggesting that different types of mechanisms operate in the Rh-catalyzed hydroamination and the present bifunctional catalysis with **2**.

Stoichiometric Reactions of Pyrazolato Complex 2. The remarkable efficiency, functional group tolerance, and product selectivity without formation of potential diastereomers and other byproducts in the intramolecular hydroamination with the bifunctional pyrazolato catalyst prompted us to explore more details of the reaction mechanism. Scheme 1 illustrates

Scheme 1. Possible Reaction Pathways for Hydroamination Catalyzed by 2[a]

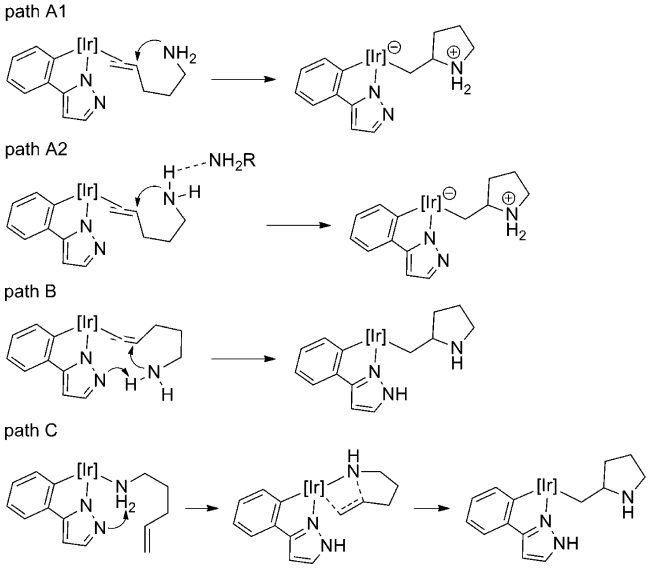

[a][Ir] = Cp*Ir.

possible key steps for the hydroamination with the pyrazolato catalyst **2**. The first two paths, A and B, include nucleophilic attack of the amino group at the olefin bond activated by coordination to the Lewis acidic iridium(III) center. Path A features the *anti* addition of the amino group and metal across the olefin bond, which is typically observed in Wacker-type heterocyclization.[22,23] Quite recently, Tobisch[24] investigated our present catalyst system computationally and proposed a modified pathway assisted by an additional amine molecule (path A2). Alternatively, nucleophilic attack of the amino group with the aid of the Brønsted basic pyrazolato ligand may be possible (path B), although that would lead to *syn* addition, which is uncommon in coordinatively saturated complexes, since such an addition is generally associated with the precoordination of the nucleophile.[25] In the last mechanism, path C, initial cleavage of the N−H bond in the substrate occurs by metal−pyrazolato cooperation and subsequent olefin insertion into the resulting metal−amido bond completes the cyclization.[26]

In order to gain further insights into the reaction mechanisms, we first investigated stoichiometric reactions of the pyrazolato-bridged dimer **2** with alkenes and amines. Exposure of a dichloromethane solution of the pyrazolato-bridged dimer **2** to ethylene (1 atm) resulted in the formation of the pyrazolato−ethylene complex **8**, as shown in Scheme 2.

Scheme 2. Stoichiometric Reactions of 2

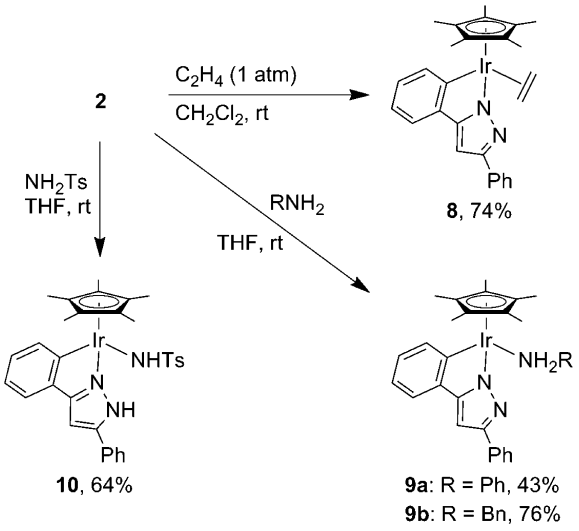

The ^{13}C{^{1}H} NMR spectrum of **8** exhibited a signal ascribed to the coordinated ethylene at δ 48.8, which is typical for Ir(III) ethylene complexes.[27] The C═C bond length in **8** (1.389(10) Å), measured by X-ray analysis (Figure 2), is only slightly longer than that of free alkenes (1.335 Å),[28] suggesting that π back-donation to the ethylene is not dominant and the ligated ethylene is potentially electrophilic. We also found that the ethylene complex **8** serves as a catalyst precursor almost as efficiently as the pyrazolato-bridged dimer **2**, indicating that the ethylene ligand is sufficiently labile. For example, intramolecular hydroamination of the aminoalkene **3a** with **8** instead of **2** under conditions otherwise identical with those in entry 1 of Table 1 afforded the cyclization product **4a** in 82% NMR yield.

On the other hand, when **2** was treated with aniline and benzylamine, the corresponding amine complexes **9** were obtained (Scheme 2). In the ^{1}H NMR spectra of **9**, broad

dx.doi.org/10.1021/om301063n | *Organometallics* 2012, 31, 8444−8455

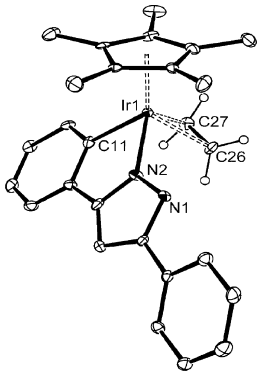

Figure 2. Structure of **8**. One of the two crystallographically independent molecules is shown. Hydrogen atoms, except for those in the ethylene ligand, are omitted for clarity.

resonances assignable to the amine protons appear in the range δ 2−5. The crystal structures of these amine complexes are depicted in Figure 3. In both crystals, a solvated water molecule

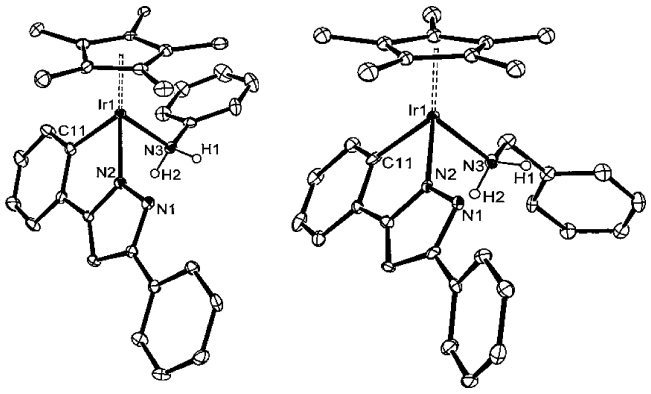

Figure 3. Structures of **9a** (left) and **9b** (right). For **9a**, one of the two crystallographically independent molecules is shown. Hydrogen atoms, except for the amine protons, are omitted for clarity.

links two molecules of the amine complexes through N(pyrazolato)···H_2O and RNH_2···OH_2 hydrogen bonds with four short N···O distances ranging from 2.804(5) to 2.984(5) Å, indicating the Brønsted acidic/basic nature of the amine and pyrazolato ligands.

Isolation of **9** demonstrated that the chelating pyrazole is more acidic than the coordinated amines. The order of acidity is, however, delicately affected by a subtle change of the substituents. In fact, treatment of **2** with *p*-toluenesulfonamide led to the formation of the sulfonamidato−pyrazole complex **10**, as shown in Scheme 2. The ^{1}H NMR spectrum of **10** displays a characteristic low-field resonance due to the pyrazole NH group at δ 10.46 as well as the sulfonamidato NH singlet at δ 2.17. The detailed structure of **10** has been determined by X-ray analysis (Figure 4). The pyrazole ligand is engaged in intermolecular hydrogen bonding with a sulfonyl oxygen atom in a neighboring molecule, forming a one-dimensional infinite chain. Protonation of the pyrazolato ligand is also deduced from the larger N(α)−N(β)−C angle (109.7°, mean of the two crystallographically independent molecules);[15] the corresponding angles in the pyrazolato complexes **9** are 105.9° (**9a**, mean) and 105.4(4)° (**9b**). Formation of the pyrazole complex **10** manifests a facile proton shift between the amine substrate and the cooperating pyrazolato ligand. In addition to the

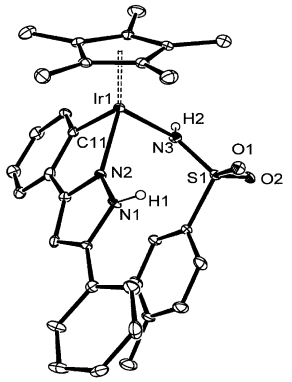

Figure 4. Structure of **10**. One of the two crystallographically independent molecules is shown. Hydrogen atoms, except for the NH protons, are omitted for clarity.

preparation of the *N*-methyl complex as shown in eq 2, the reaction provides an example of bond cleavage by acid/base bifunctional complexes, which has been established in the reactions of bifunctional amido complexes with various Brønsted acidic organic compounds, including nitromethane, terminal alkynes, and malonates.[26,29]

We also monitored the reaction of the catalyst precursor **2** and the less reactive aminoalkene substrate **3b** by ^{1}H NMR spectroscopy (Scheme 3). After 22 h at room temperature,

Scheme 3. Reaction of 2 with 3b

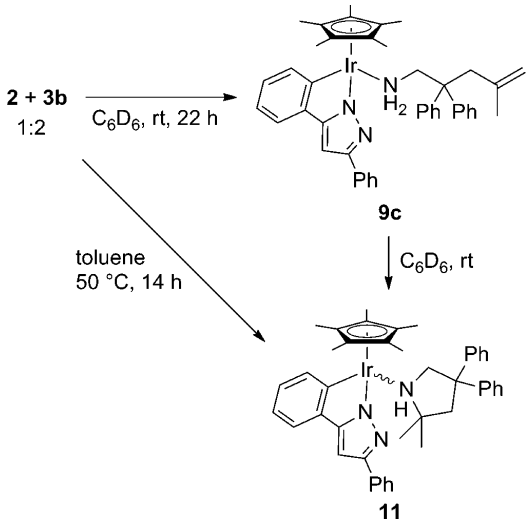

signals assignable to the amine complex **9c** appeared in the spectrum, which illustrates the diastereotopic nature of the amine protons as observed in the benzylamine complex **9b**. A prolonged reaction led to slow conversion of **9c** into a 1:1 mixture of the pyrrolidine complexes **11**, which was also obtained more conveniently by the reaction of **2** and **3b** in toluene at 50 °C. An X-ray analysis revealed that the mixture contains one of the two possible diastereomers (**11a**) with two stereogenic centers, the iridium and amine nitrogen atoms (Figure 5). Since the ^{1}H NMR signals of the two products are closely related to each other, we assigned the other product **11b** as the diastereomer of **11a**.

Because the observation of **8**−**11** indicates that both olefin and amine activation pathways are plausible, we next estimated the stability of the intermediates assumed in Scheme 1 by DFT

dx.doi.org/10.1021/om301063n | *Organometallics* 2012, 31, 8444−8455

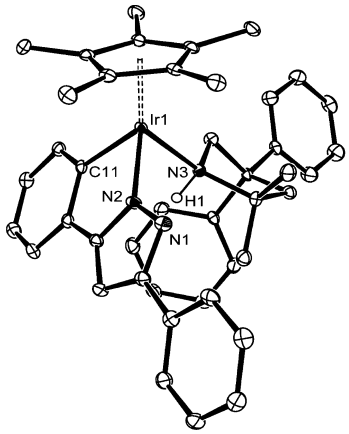

Figure 5. Structure of **11a**. Hydrogen atoms, except for the amine proton, are omitted for clarity.

calculations. Chart 2 shows the scrutinized species, which are derived from the secondary aminoalkene **3d**, with their

Chart 2. Calculated Relative Free Energies of Assumed Intermediates

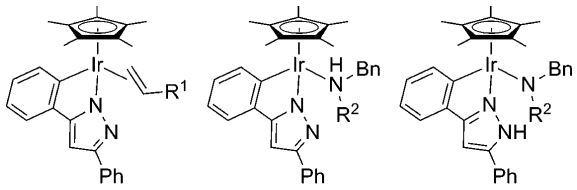

calculated relative free energies. The olefin complex **A** proved to be more stable than the amine complex **B**, a congener of the experimentally observed **9c**, by 14.9 kcal mol^{-1}, suggesting that both species are likely to be present in the catalytic cycle as resting states or intermediates. On the other hand, the much higher energy of the pyrazole–amido complex **C** contradicts path C, the N–H activation of the Brønsted basic alkylamine substrates.

Synthesis and Properties of Pyrazole–Alkyl Complex. The possible mechanisms shown in Scheme 1 all involve (alkyl)iridium species arising from the C–N bond formation step. To explore the nature of the metal–alkyl bond, we synthesized an alkyl complex bearing a protic pyrazole ligand. Treatment of the chlorido complex **1** with 0.5 equiv of dimethylzinc resulted in the formation of the pyrazole–methyl complex **12** along with a small amount of uncharacterized byproduct (eq 3).[30] The ^{1}H NMR spectrum of **12** features a

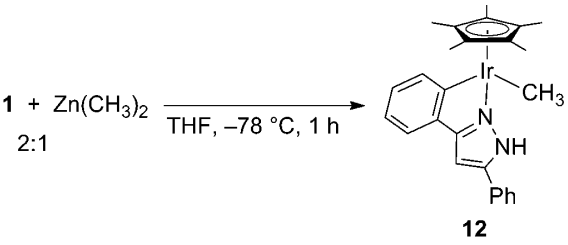

(3)

high-field methyl singlet at δ −0.27 as well as a β-NH resonance at δ 9.56. Isolation of **12** was, however, hampered by slow decomposition during recrystallization in toluene–hexane, even at −30 °C. Although the decomposition product has eluded full identification, the ^{1}H NMR spectrum indicated loss of the methyl ligand and retention of the pyrazole proton (δ 10.28). Importantly, the pyrazolato-bridged dimer **2** was not observed. The result may imply that direct proton transfer from the pyrazole to the alkyl ligand is unfeasible, although the behavior of **12** does not necessarily represent the nature of the (alkyl)iridium intermediate. The pyrrolidine moiety and the metal center in the aminoalkyl intermediate as well as external substrate/product amine molecules may be involved in the proton relay in the catalytic hydroamination.[9,24,31]

Kinetic Experiments. We then carried out a series of kinetic experiments to draw a clear picture of the reaction mechanism. Since the insufficient solubility of the pyrazolato-bridged dimer **2** prevented precise control of the catalyst concentration, we used the ethylene complex **8**, which also produces the catalytically active mononuclear pyrazolato species (vide supra), as the catalyst precursor. We first monitored consumption of the aminoalkene **3d** in the presence of a catalytic amount of **8** by ^{1}H NMR spectroscopy (Figure 6).

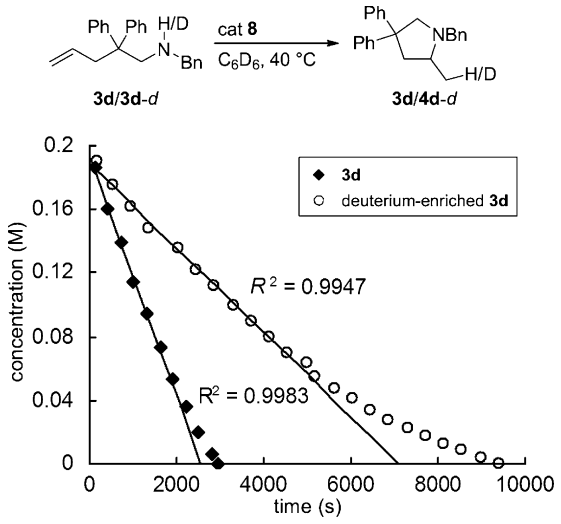

Figure 6. Profile for the decay of secondary aminoalkenes **3d** and **3d**-*d* in the presence of **8**. Reaction conditions: **3d**:Ir = 20:1, [**3d**] = 0.20 M, 40 °C, in C_6D_6.

The reaction obeyed zero-order kinetics with regard to the concentration of the aminoalkene until about 65% conversion, and consequently the substrate coordination step to the iridium center should be relatively fast. The apparent rate constant k_{obs} at the early stage of the reaction with an $[Ir]_0$ value of 0.010 M at 40 °C was determined to be 7.54×10^{-5} M s^{-1}. When the deuterium-enriched aminoalkene **3d** (ca. 60% D) was subjected to the catalytic cyclization, the reaction rate significantly decreased, as illustrated in Figure 6. The k_{obs} value of the deuteriated substrate (2.65×10^{-5} M s^{-1}) is much smaller than that of the nondeuteriated aminoalkene **3d**, and the k_H/k_D ratio is thus estimated to be more than 2.8.

On the other hand, the reaction rate exhibited approximate first-order dependence on the initial concentration of the catalyst $[Ir]_0$, as shown in Figure 7. The deviation of the plot from linearity may be explained by an equilibrium between the catalytically active mononuclear pyrazolato species and the

dx.doi.org/10.1021/om301063n | Organometallics 2012, 31, 8444–8455

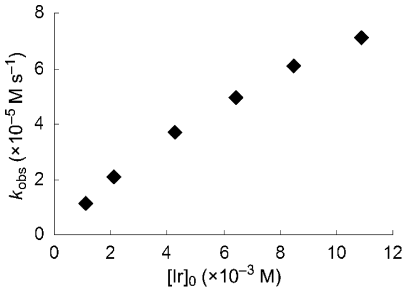

Figure 7. Plot of k_{obs} versus $[Ir]_0$ in hydroamination of **3d** in the presence of various amounts of **8**. Reaction conditions: **3d**:Ir = 20–200, [**3d**] = 0.22 M, 40 °C, in C_6D_6.

dimerized resting state **2**, which would shift to the latter as the concentration of the iridium complexes increases.

The reaction rates of the cyclization of **3d** were determined at temperatures ranging from 30 to 60 °C. The Arrhenius and Eyring plots shown in Figure 8 provided an activation energy of

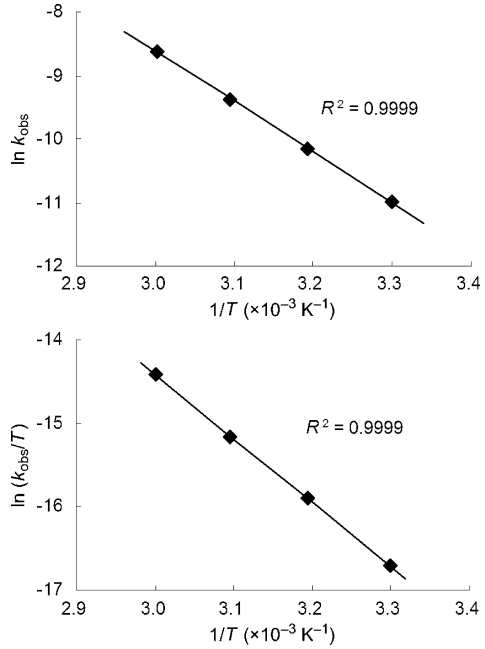

Figure 8. Arrhenius plot (above) and Eyring plot (below) for the hydroamination of **3d** catalyzed by **8**. The reactions were conducted at a temperature range of 30–60 °C. Reaction conditions: **3d**:Ir = 50:1, [**3d**] = 0.23 M, in C_6D_6.

E_a = 15.9 kcal mol^{-1}, an activation enthalpy of $\Delta H^{\ddagger}$ = 15.2 kcal mol^{-1}, and an activation entropy of $\Delta S^{\ddagger}$ = −30 cal mol^{-1} K^{-1}. This large negative $\Delta S^{\ddagger}$ value suggests a highly ordered transition state in the rate-determining step.

Computational Study of Protonolysis Step. Given that the cyclization step is rate-determining, the observed primary KIE of the NH proton and the zero-order rate dependence of the substrate concentration are best explained by path B in Scheme 1. An alternative scenario that merits discussion is one involving rate-determining protonolysis of the (alkyl)iridium species which results from the cyclization. Stradiotto and co-workers revealed similar primary KIE (3.4(3)) and $\Delta S^{\ddagger}$ values (−23.1(8) cal mol^{-1} K^{-1}) in $[IrCl(cod)]_2$-catalyzed intramolecular hydroamination, and with the aid of DFT calculations, they concluded that reductive elimination from an (alkyl)(hydrido)iridium(III) intermediate, which is generated by cyclization and subsequent proton migration, is rate-determining.[9] The large negative activation entropy value was ascribed to a highly ordered transition-state structure in the reductive elimination, although the actual $\Delta S^{\ddagger}$ values for reductive elimination reported in the literature fall in both the positive and negative ranges.[32] Tobisch[24] also proposed that protonolysis of the (alkyl)iridium species in our present bifunctional catalysis involves turnover-limiting reductive elimination from an (alkyl)(hydrido)iridium(V) intermediate after proton migration assisted by external amine molecules. We therefore estimated the thermodynamic parameters in the reductive elimination from the (*tert*-aminoalkyl)(hydrido)-iridium(V) intermediate by DFT calculations (Scheme 4). The slightly positive $\Delta S^{\ddagger}$ value thus obtained is inconsistent with the result of the kinetic experiments, indicating that the reductive elimination stage is not rate-determining.

Proposed Mechanism of Catalytic Hydroamination. The accumulated data led to the following mechanistic considerations. The DFT calculations exclude the primary N–H cleavage (path C in Scheme 1) and rate-determining protonolysis of the (alkyl)iridium species. The zero-order rate dependence on substrate concentration indicates that the initial olefin coordination as well as assistance of the external amine (path A2) is not involved in the turnover-limiting step. Therefore, the cyclization stage is most likely to be the rate-determining step. Since path A1 is against the observed primary KIE of the NH proton, we conclude that the path B is the most probable mechanistic scenario. The *syn* addition therein may further be implied by the stereochemical outcome in the cyclization of **3n**, which is different from the result in the

Scheme 4. Calculated Activation Parameters for the Reductive Elimination Step

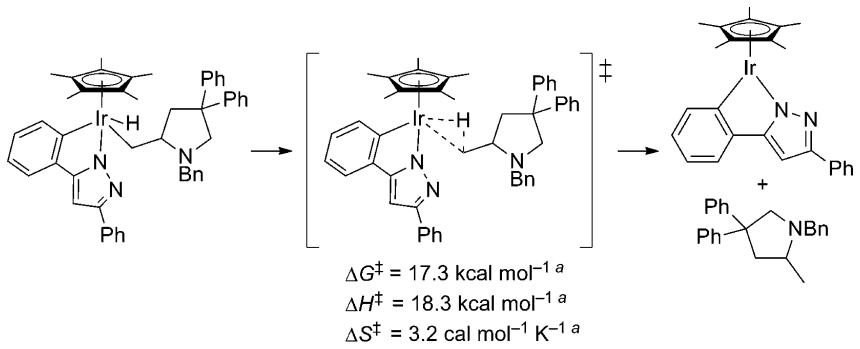

[a]Values relative to that of the olefin complex **A** in Chart 2.

dx.doi.org/10.1021/om301063n | *Organometallics* 2012, 31, 8444–8455

rhodium−biarylphosphine catalyst (vide supra),[6] for which an *anti* addition mechanism has been proposed.[10] Unfortunately, conclusive experiments to distinguish the two stereochemical courses using appropriately designed internal aminoalkenes[10,33] were hampered by the low catalytic activity of **2** toward such substrates.

The overall mechanism for the intramolecular hydroamination catalyzed by the bifunctional pyrazolato complex is illustrated in Scheme 5. The coordinatively unsaturated

Scheme 5. Proposed Mechanism of the Intramolecular Hydroamination Catalyzed by 2

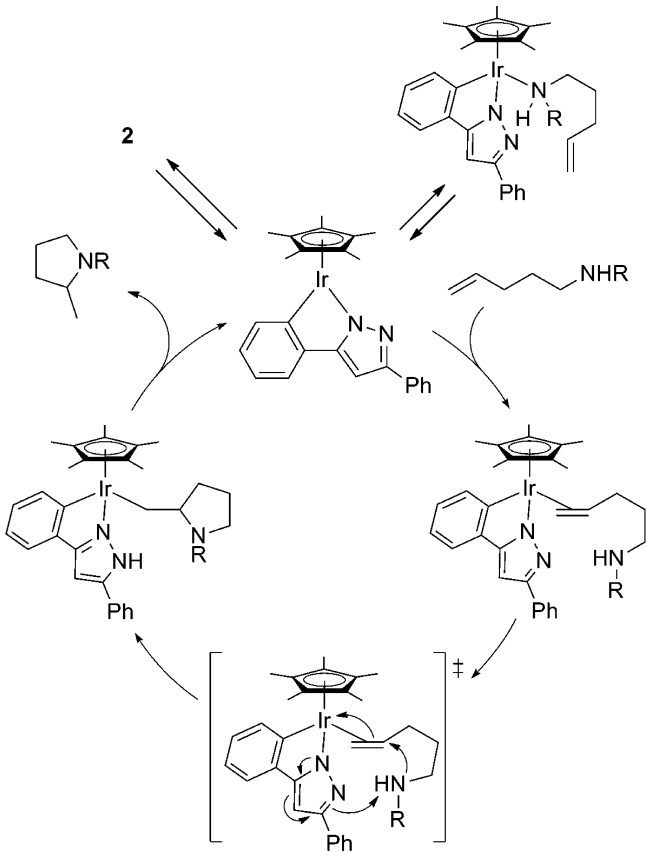

pyrazolato complex, which would be in equilibrium with the dimer **2**, first reacts with the substrate aminoalkene to form an olefin-bound or amine-bound complex. The experimentally observed latter complex is a resting state. The coordinated olefin in the former then undergoes rate-determining nucleophilic attack of the amino group from the same side as the metal, which is assisted by the concurrent deprotonation of the amino group with the pyrazolato ligand. The sterically constrained transition state involving N−H bond cleavage agrees with the observed negative activation entropy and primary KIE. The multiple noncovalent interactions between the bifunctional pyrazolato catalyst and the substrate in the transition state may be responsible for the high stereoselectivity in the catalysis. A subsequent proton shift in the resulting alkyl−pyrazole complex affords the cyclization product and regenerates the unsaturated pyrazolato complex. The coordinative saturation of the alkyl intermediate would inhibit the competing β-elimination that leads to undesired oxidative amination.[22,34] This final protonolysis step seems, however, not so straightforward when considering the decomposition of the methyl−pyrazole complex **12**, yielding no pyrazolato-bridged dimer **2**; apparently, more complicated proton migration should take place. On the basis of comprehensive DFT calculations, Tobisch[23] recently proposed a distinct mechanism featuring nucleophilic *anti* addition (path A2 in Scheme 1) and rate-determining reductive elimination from a (hydrido)iridium(V) intermediate. However, this mechanism seems inconsistent with the markedly negative $\Delta S^{\ddagger}$ value observed. The discrepancy may be ascribed to the difference in the aminoalkenes under consideration: our kinetic experiments were carried out for the secondary aminoalkene **3d**, while Tobisch used a less hindered primary aminoalkene, wherein the hydrogen-bonding stabilization with the external amine substrate may be overestimated.

CONCLUSION

We have demonstrated that the bifunctional iridium pyrazolato complex **2** is an efficient, functional-group-tolerant intramolecular hydroamination catalyst for aminoalkenes. A series of stoichiometric reactions and kinetic experiments of the pyrazolato complexes as well as theoretical calculations are fully consistent with the unprecedented metal−ligand bifunctional mechanism,[35] in which the Lewis acidic metal and the Brønsted basic pyrazolato ligand cooperatively activate the olefin and amino groups of the substrate in the rate-determining transition state (Scheme 4). Owing to the multipoint binding of the substrate delicately controlled by the cooperating ligand, the bifunctional pyrazolato catalyst is applicable to less reactive aminoalkenes bearing a primary amino group or without *gem* substituents on the linker chain. The tight-fitting assembly of the catalyst and substrate in the transition state also contribute to the perfect diastereoselectivity in the hydroamination of aminoalkenes bearing allylic substituents. In addition, intermediacy of the coordinatively saturated alkyl species would result in the excellent selectivity of hydroamination over oxidative amination arising from β-elimination. Use of the metal−ligand cooperating bifunctional catalyst thus provided a novel strategy in hydroamination, which will guide the future development of increasingly effective catalysts.

EXPERIMENTAL SECTION

General Procedures. All manipulations were performed under an atmosphere of argon using standard Schlenk techniques unless otherwise specified. Solvents were dried by refluxing over sodium benzophenone ketyl (THF, toluene, C_6D_6, diethyl ether, and hexane) or CaH_2 (CH_2Cl_2) and distilled before use. Reagents were purchased from Kanto Chemicals, Aldrich, and Tokyo Chemical Industry and used as received. Silica gel column chromatography was performed using Fuji Silysia silica gel FL100D. Automated silica gel column chromatography was performed using a Yamazen YFLC AI-580 instrument with a Yamazen Hi-Flash column. ^{1}H (399.78 MHz) and ^{13}C (100.53 MHz) NMR spectra were obtained on a JEOL JNM-ECX400 spectrometer. ^{1}H NMR shifts are relative to the signal of the residual protiated solvent: $CHCl_3$, δ 7.26; C_6D_5H, δ 7.15. $^{13}C\{^1H\}$ NMR shifts are relative to the signal of the solvent: $CDCl_3$, δ 77.0. IR spectra were recorded on a JASCO FT/IR-610 spectrometer. Elemental analyses were performed on a Perkin-Elmer 2400II CHN analyzer. HRMS spectra were recorded on a Bruker Daltonics micrOTOF II spectrometer. The pyrazole complex **1**[17] and the pyrazolato complex **2**[17] as well as aminoalkenes **3a**,[36] **3c**,[8b] **3d**,[8b] **3e**,[3a] **3g**,[37] **3h**,[6] **3i**,[8a] **3k**,[8b] **3l**,[8b] **3m**,[8b] and **3n**[6] were prepared according to the literature.

Synthetic Details. *Synthesis of 4-Methyl-2,2-diphenylpent-4-en-1-amine (**3b**).* This compound was synthesized in a manner similar to that for the synthesis of **3a**[35] using diphenylacetonitrile and 3-chloro-2-

dx.doi.org/10.1021/om301063n | *Organometallics* 2012, 31, 8444−8455

methylprop-1-ene as starting materials and identified according to the reported spectroscopic data.[6] ^{1}H NMR (δ, $CDCl_3$): 1.07 (s, 3H, CH_3), 2.92 (s, 2H, CH_2=C(CH_3)CH_2), 3.41 (s, 2H, CH_2NH_2), 4.59, 4.82 (m, 1H each, CH_2=C(CH_3)), 7.16−7.20 (m, 6H, C_6H_5), 7.25−7.29 (m, 4H, C_6H_5).

*Synthesis of 3-Methyl-2,2-diphenylpent-4-en-1-amine (**3f**).* This compound was synthesized by a regioselective Tsuji−Trost reaction[38] with some modifications. To a suspension of NaH (60 wt % in mineral oil, 207.9 mg, 5.20 mmol) in THF (10 mL) was added diphenylacetonitrile (869.9 mg, 4.502 mmol), and the mixture was stirred for 1 h at 0 °C before diluted with THF (40 mL). Separately, a solution of $[PdCl(\eta^3\text{-crotyl})]_2$[39] (29.5 mg, 0.0749 mmol) and PBu^t_3 (73 μL, 0.30 mmol) in THF (6 mL) was stirred for 30 min at room temperature. After addition of but-3-en-2-yl acetate (0.38 mL, 3.0 mmol) to the catalyst solution, this mixture was added to the solution prepared first. The resulting solution was stirred for 16 h, during which time the temperature was gradually increased from 0 °C to room temperature. Water (20 mL) was added to the solution, and the mixture was extracted with ethyl acetate (20 mL). The organic phase was washed with saturated aqueous NH_4Cl solution and brine (20 mL, respectively) and dried with $MgSO_4$, and the solvents were removed in vacuo. Purification by automatic silica gel column chromatography with gradually increasing amounts of ethyl acetate in hexane (from 0% to 13% v/v) as eluent gave 3-methyl-2,2-diphenylpent-4-enenitrile as a colorless oil (0.7441 g, 3.009 mmol, 100%). ^{1}H NMR (δ, $CDCl_3$): 1.19 (d, $^3J_{HH}$ = 6.7 Hz, 3H, CH_3), 3.45 (pseudo quint, 1H, CH_2=CHC*H*(CH_3)), 5.05−5.13 (m, 2H, CH_2=CH), 5.83 (ddd, $^3J_{HH}$ = 18.0, 10.4, 7.6 Hz, 1H, CH_2=C*H*), 7.21−7.40 (m, 6H, C_6H_5), 7.47−7.52 (m, 4H, C_6H_5).

To a suspension of $LiAlH_4$ (285.0 mg, 7.510 mmol) in dehydrated diethyl ether (8 mL) was added 3-methyl-2,2-diphenylpent-4-enenitrile (0.7441 g, 3.009 mmol) at 0 °C, and the mixture was refluxed for 17 h at 50 °C. After dilution with diethyl ether (15 mL), the reaction was quenched by slow addition of $Na_2SO_4{\cdot}10H_2O$ at 0 °C and the mixture was stirred at room temperature. The resulting white precipitate was filtered off and extracted with diethyl ether (ca. 50 mL). Evaporation of the solvent in vacuo gave a colorless oil, which was purified by bulb-to-bulb distillation to give 3-methyl-2,2-diphenylpent-4-en-1-amine (657.1 mg, 2.614 mmol, 87%). ^{1}H NMR (δ, $CDCl_3$): 0.93 (d, $^3J_{HH}$ = 6.7 Hz, 3H, CH_3), 3.26 (AB pattern, 2H, CH_2NH_2), 3.27 (m, 1H, CH_2=CHC*H*(CH_3)), 4.98−5.01, 5.07−5.11 (m, 1H each, CH_2=CH), 5.43 (ddd, $^3J_{HH}$ = 18.6, 10.1, 8.6 Hz, 1H, CH_2=C*H*), 7.17−7.34 (m, 10H, C_6H_5).

To a solution of 3-methyl-2,2-diphenylpent-4-en-1-amine (657.1 mg, 2.614 mmol) in methanol (7 mL) was added benzaldehyde (0.28 mL. 2.8 mmol), and the solution was stirred for 4 h at room temperature in air. Then the solution was treated with $NaBH_4$ (148 mg, 3.91 mmol) and stirred for 15 h at room temperature. The resulting mixture was treated with water (20 mL) and 1 M NaOH solution (7 mL) and extracted with CH_2Cl_2 (3 × 15 mL). The combined organic layer was dried with $MgSO_4$, and the solvents were removed in vacuo. Purification by automated silica gel column chromatography with gradually increasing amounts of ethyl acetate in hexane (from 0% to 15% v/v) as eluent gave **3f** as a colorless oil (658.7 mg, 1.929 mmol, 74%). ^{1}H NMR (δ, $CDCl_3$): 0.90 (d, $^3J_{HH}$ = 7.0 Hz, 3H, CH_3), 3.15 (AB pattern, 2H, CPh_2CH_2NH), 3.53 (pseudo quint, 1H, CH_2=CHC*H*(CH_3)), 3.62 (AB pattern, 2H, $NHCH_2Ph$), 4.92−4.95, 5.03−5.08 (m, 1H each, CH_2=CH), 5.44 (ddd, $^3J_{HH}$ = 18.6, 10.1, 8.6 Hz, 1H, CH_2=C*H*), 7.11−7.29 (m, 15H, C_6H_5). $^{13}C\{^1H\}$ NMR (δ, $CDCl_3$):16.6, 40.5, 54.1, 54.7, 57.5, 115.1, 125.98, 126.04, 126.6, 127.1, 127.5, 127.8, 128.1, 129.7, 130.1, 140.7, 141.2, 143.1, 144.2. Anal. Calcd for $C_{25}H_{27}N$: C, 87.93; H, 7.97; N, 4.10. Found: C, 88.00; H, 7.93; N, 4.11.

*Synthesis of 2,2-Diphenylhex-4-en-1-amine (**3j**).* This compound was synthesized in a manner similar to that for the synthesis of **3a**[35] using diphenylacetonitrile and 1-chlorobut-2-ene (mixture of *E* and *Z* isomers) as starting materials and identified according to the reported spectroscopic data.[40] Data for the *E* isomer are as follows. ^{1}H NMR (δ, $CDCl_3$): 1.56 (dd, $^3J_{HH}$ = 6.4 Hz, $^4J_{HH}$ = 1.2 Hz, 3H, CH_3), 2.83 (d, $^3J_{HH}$ = 7.0 Hz, 2H, CH=CHC*H*$_2$), 5.01 (m, 1H, CH=C*H*CH$_2$), 5.45 (m, 1H, C*H*=CHCH$_2$), 7.15−7.30 (m, 10H, C_6H_5). $^{13}C\{^1H\}$ NMR (δ, $CDCl_3$): 18.0, 39.8, 48.5, 51.6, 125.9, 126.7, 128.0, 128.2, 146.4. Data for the *Z* isomer are as follows. ^{1}H NMR (δ, $CDCl_3$): 1.51 (dd, $^3J_{HH}$ = 6.7 Hz, $^4J_{HH}$ = 1.5 Hz, 3H, CH_3), 2.90 (d, $^3J_{HH}$ = 7.3 Hz, 2H, CH=CHC*H*$_2$), 5.08 (m, 1H, CH=C*H*CH$_2$), 5.45 (m, 1H, C*H*=CHCH$_2$), 7.15−7.30 (m, 10H, C_6H_5). $^{13}C\{^1H\}$ NMR (δ, $CDCl_3$): 12.9, 33.9, 49.0, 51.9, 126.0, 126.4, 128.3, 146.3. The signals of olefin and phenyl carbon atoms were not fully assigned due to the overlap.

*Synthesis of **5**.* To a suspension of **2** (43.8 mg, 40.1 μmol) in THF (4 mL) was added CH_3I (5.00 μL, 80.3 μmol), and the mixture was stirred for 16 h at room temperature. After removal of the solvent in vacuo, the resulting solid was recrystallized from THF/hexane (1 mL/20 mL) to give **5** as red crystals (23.8 mg, 34.6 μmol, 43%). ^{1}H NMR (δ, $CDCl_3$): 1.81 (s, 15H, $C_5(CH_3)_5$), 3.98 (s, 3H, NCH_3), 6.56 (s, 1H, aryl), 6.96, 7.08 (m, 1H each, aryl), 7.42−7.52 (m, 6H, aryl), 7.72 (m, 1H, aryl). Anal. Calcd for $C_{26}H_{28}IIrN_2$: C, 45.41; H, 4.10; N, 4.07. Found: C, 45.71; H, 4.30; N, 3.95.

*Synthesis of **8**.* A solution of **2** (49.8 mg, 45.6 μmol) in dichloromethane (4 mL) was degassed by three freeze−pump−thaw cycles. C_2H_4 (1 atm) was introduced, and the mixture was stirred for 40 min at room temperature. After removal of the solvent in vacuo, the resulting solid was dissolved in diethyl ether (1 mL). Addition of hexane (20 mL) to the solution gave **8** as ocher solids (13.0 mg, 22.7 μmol, 25%). The mother liquid was concentrated to dryness, and the resulting solid was dissolved in hexane (ca. 5 mL). Cooling of the solution to −30 °C afforded additional **8**; the combined yield was 25.6 mg (44.6 μmol, 74%). ^{1}H NMR (δ, $CDCl_3$): 1.70 (s, 15H, $C_5(CH_3)_5$), 2.98, 3.04 (m, 2H each, C_2H_4), 6.53 (s, 1H, aryl), 6.91, 7.04, 7.17 (m, 1H each, aryl), 7.33−7.41 (m, 4H, aryl), 7.88 (m, 2H, aryl). $^{13}C\{^1H\}$ NMR (δ, $CDCl_3$): 8.2, 48.8, 95.0, 98.3, 120.3, 123.6, 125.0, 125.7, 128.2, 135.9, 136.3, 141.3, 147.9, 153.1, 157.7. Anal. Calcd for $C_{27}H_{29}IrN_2$: C, 56.52; H, 5.09; N, 4.88. Found: C, 56.77; H, 5.24; N, 4.87. Recrystallization of the solid from diethyl ether at −30 °C gave the ether adduct **8**·Et_2O as yellow crystals suitable for X-ray analysis.

*Synthesis of **9a**·0.5H_2O.* To a suspension of **2** (40.0 mg, 36.7 μmol) in THF (3 mL) was added aniline (6.70 μL, 73.4 μmol), and the mixture was stirred for 12 h at room temperature. After removal of the solvent in vacuo, the resulting solid was recrystallized from THF/hexane (0.5 mL/20 mL) to give **9a**·0.5H_2O as yellow-green crystals (20.3 mg, 31.8 μmol, 43%). ^{1}H NMR ($CDCl_3$): δ 1.52 (s, 15H, $C_5(CH_3)_5$), 4.30 (br, 2H, NH_2), 6.66 (s, 1H, aryl), 6.88, 7.00 (m, 2H each, aryl), 7.11 (m, 1H, aryl), 7.21 (m, 3H, aryl), 7.39 (m, 2H, aryl), 7.51 (m, 1H, aryl), 7.77 (m, 1H, aryl), 7.96 (m, 2H, aryl). Anal. Calcd for $C_{31}H_{33}IrN_3O_{0.5}$: C, 57.47; H, 5.13; N, 6.49. Found: C, 57.34; H, 5.37; N, 6.41.

*Synthesis of **9b**·0.5H_2O.* To a suspension of **2** (47.5 mg, 43.5 μmol) in THF (4 mL) was added benzylamine (9.50 μL, 86.9 μmol), and the mixture was stirred for 1 h at room temperature. After removal of the solvent in vacuo, the resulting solid was recrystallized from dichloromethane/hexane (1 mL/20 mL) with a drop of water to give **9b**·0.5H_2O as yellow crystals (43.8 mg, 66.2 μmol, 76%). ^{1}H NMR (δ, $CDCl_3$): 1.85 (s, 15H, $C_5(CH_3)_5$), 2.41, 3.35 (br, 1H each, NH_2), 3.56 (m, 2H, CH_2), 6.62 (s, 1H, aryl), 6.79 (m, 2H, aryl), 6.96, 7.08 (m, 1H each, aryl), 7.13−7.18 (m, 3H, aryl), 7.33 (m, 3H, aryl), 7.48, 7.69 (m, 1H each, aryl), 7.91 (m, 2H, aryl). Anal. Calcd for $C_{32}H_{35}IrN_3O_{0.5}$: C, 58.07; H, 5.33; N, 6.35. Found: C, 58.20; H, 5.09; N, 6.33.

*Synthesis of **10**.* To a suspension of **2** (39.8 mg, 36.5 μmol) in THF (3 mL) was added $TsNH_2$ (12.5 mg, 73.0 μmol), and the mixture was stirred for 4 h at room temperature. After removal of the solvent in vacuo, the resulting solid was recrystallized from dichloromethane/hexane (1 mL/20 mL) to give **10** as orange crystals (33.3 mg, 46.4 μmol, 64%). ^{1}H NMR (δ, $CDCl_3$): 1.78 (s, 15H, $C_5(CH_3)_5$), 2.14 (s, 3H, $C_6H_4CH_3$), 2.17 (s, 1H, NHTs), 6.18 (s, 1H, aryl), 6.61, 6.81 (d, $^3J_{HH}$ = 8.1 Hz, 2H each, $SO_2C_6H_4$), 7.07, 7.12 (m, 1H each, aryl), 7.34−7.47 (m, 6H, aryl), 7.72 (m, 1H, aryl), 10.46 (br, 1H, aryl-NH). Anal. Calcd for $C_{32}H_{34}IrN_3O_2S$: C, 53.61; H, 4.78; N, 5.86. Found: C, 53.36; H, 4.90; N, 5.89.

*Reaction of **2** with 4-Methyl-2,2-diphenylpent-4-en-1-amine (**3b**).* In an NMR tube equipped with a J. Young valve were added

dx.doi.org/10.1021/om301063n | *Organometallics* 2012, 31, 8444−8455

3b (3.8 mg, 15 μmol), **2** (8.1 mg, 7.4 μmol), and C_6D_6 (0.5 mL). The mixture was maintained at room temperature and monitored by ^{1}H NMR. After 22 h, signals assigned to the amine complex **9c** were observed. ^{1}H NMR (δ, C_6D_6): 0.77 (s, 3H, CH_2=C(CH_3)), 1.46 (s, 15H, $C_5(CH_3)_5$), 2.14 (AB pattern, 2H, CH_2=C(CH_3)CH_2), 2.28, 2.52 (br t, 1H each, NH_2), 2.87, 3.00 (m, 1H each, CH_2NH_2), 4.08 (s, 1H, CH_2=C(CH_3)), 4.63 (d, $^2J_{HH}$ = 1.5 Hz, 1H, CH_2=C(CH_3)), 6.61 (m, 4H, aryl), 6.90 (m, 6H, aryl), 6.96 (s, 1H, aryl), 7.16 (m, 2H, aryl), 7.27 (m, 1H, aryl), 7.38 (m, 2H, aryl), 7.73, 7.79 (m, 1H each, aryl), 8.36 (m, 2H, aryl). The connectivity of the protons was confirmed by a ^{1}H–^{1}H COSY analysis.

Synthesis of ***11****.* To a solution of **3b** (17.9 mg, 71.2 μmol) in toluene (2 mL) was added **2** (38.7 mg, 35.5 μmol), and the mixture was stirred for 14 h at 50 °C. After removal of the solvent under reduced pressure, the resulting solid was recrystallized from diethyl ether/hexane (2 mL/20 mL) to give yellow crystals of **11** as a 1:1 mixture of the diastereomers (22.7 mg, 28.5 μmol, 40%). ^{1}H NMR (δ, $CDCl_3$): −0.32, −0.24 (s, 3H each, $C(CH_3)_2$), 1.20, 1.47 (s, 3H each, $C(CH_3)_2$), 1.74, 1.75 (s, 15H each, $C_5(CH_3)_5$), 2.34 (pseudo t, 2H, $C(CH_3)_2CH_2CPh_2$), 2.52 (m, 2H, $C(CH_3)_2CH_2CPh_2$), 2.90 (d, $^2J_{HH}$ = 12.5 Hz, 1H, $NHCH_2CPh_2$), 3.06 (d, $^2J_{HH}$ = 12.8 Hz, 1H, $NHCH_2CPh_2$), 2.91, 3.05 (m, 1H each, NH), 4.09 (d, $^2J_{HH}$ = 12.5 Hz, 1H, $NHCH_2CPh_2$), 4.78 ($^2J_{HH}$ = 12.8 Hz, 1H, $NHCH_2CPh_2$), 6.47 (s, 1H, aryl), 6.59 (m, 2H, aryl), 6.66 (s, 1H, aryl), 6.72 (m, 2H, aryl), 6.80–6.95 (m, 8H, aryl), 7.04–7.33 (m, 17H, aryl), 7.42 (m, 3H, aryl), 7.70 (m, 1H, aryl), 7.90 (m, 2H, aryl), 7.94 (m, 1H, aryl), 8.13 (m, 2H, aryl). Anal. Calcd for $C_{43}H_{46}IrN_3$: C, 64.80; H, 5.82; N, 5.27. Found: C, 64.77; H, 6.00; N, 5.38.

Synthesis of ***12****.* To a solution of **1** (50.0 mg, 85.9 μmol) in THF (4 mL) was added a solution of dimethylzinc (47 μL, 0.92 M in hexane) at −78 °C, and the mixture was stirred for 1 h at −78 °C. After removal of the solvent in vacuo, the resulting solid was extracted with toluene (3 × 2 mL), and the extracts were evaporated to dryness. A ^{1}H NMR analysis of the product indicated the generation of **12** with a small amount of uncharacterized byproduct(s). ^{1}H NMR (δ, CD_2Cl_2): −0.27 (s, 3H, $IrCH_3$), 1.84 (s, 15H, $C_5(CH_3)_5$), 6.83 (d, J_{HH} = 2.1 Hz, 1 H, aryl), 6.95 (m, 2H, aryl), 7.60 (m, 2H, aryl), 9.56 (br, 1H, NH). The signals of the aryl protons were masked by those of the byproduct(s) and not fully assigned.

X-ray Diffraction Studies. Single crystals suitable for X-ray analysis were mounted on a glass fiber or on a fiber loop followed by data collection at 93 K. Diffraction experiments were performed on a Rigaku Saturn CCD area detector with graphite-monochromated Mo Kα radiation (λ = 0.710 70 Å) to a maximum 2θ value of 55°. Intensity data were corrected for Lorentz–polarization effects and for absorption. Details of crystal and data collection parameters are summarized in Table S15 (Supporting Information). Structure solution and refinements were performed with the CrystalStructure program package.[41] The heavy-atom positions were determined by a direct methods program (SIR92[42]), and the remaining non-hydrogen atoms were found by subsequent Fourier synthesis. The structures were refined against F^2 with anisotropic temperature factors for all non-hydrogen atoms unless otherwise specified. One of the two solvated diethyl ether molecules in **4f**·HBF_4·0.625Et_2O was severely disordered. The non-hydrogen atoms therein were located at two disordered positions with a total occupancy of 0.5 and included in the refinements with fixed parameters. The carbon atoms in the Cp* ligand in **9b**·0.5H_2O were refined with isotropic thermal parameters. The hydrogen atoms in the C_2H_4 ligand in **8** and solvating water molecule in **9b**·0.5H_2O were located in the difference Fourier map and refined isotropically, while the hydrogen atoms in the disordered solvating diethyl ether molecule in **4f**·HBF_4·0.625Et_2O and the solvating water molecule in **9a**·0.5H_2O were not included in the refinements. The rest of the hydrogen atoms were included in the final stages of the refinements by using a riding model.

Representative Procedure for Intramolecular Hydroamination Catalyzed by 2. To a solution of **3a** (99.3 mg, 418 μmol) in toluene (2.0 mL) was added **2** (11.4 mg, 10.4 μmol), and the mixture was stirred for 15 h at 50 °C. After removal of the solvent in vacuo, the resulting oil was chromatographed on silica gel with gradually increasing amounts of ethyl acetate in hexane (from 10% to 100% v/v) as eluent to afford **4a** (88.6 mg, 373 μmol, 89%), which gave an ^{1}H NMR spectrum in agreement with that reported in the literature.[36] Cyclic amines **4b**,[6] **4c**,[8b] **4d**,[8b] **4e**,[3a] **4g**,[37] **4h**,[6] **4i**,[8a] **4k**,[8b] **4l**,[8b] and **4m**[8b] were also identified by comparing their ^{1}H NMR spectra with those reported in the literature. Analytical data for the other hydroamination products are as follows.

*trans-N-Benzyl-2,3-dimethyl-4,4-diphenylpyrrolidine (****4f****).* ^{1}H NMR (δ, $CDCl_3$): 0.71 (d, $^3J_{HH}$ = 6.4 Hz, 3H, CH_3), 1.20 (d, $^3J_{HH}$ = 5.6 Hz, 3H, CH_3), 2.66 (m, 2H, $CHCH_3$), 3.41, 3.46 (AB pattern, 1H each, NCH_2CPh_2), 3.76, 4.10 (d, $^3J_{HH}$ = 14.0 Hz, 1H each, $PhCH_2N$), 6.94 (m, 2H, C_6H_5), 7.11–7.35 (m, 13H, C_6H_5). Colorless crystals of **4f**·HBF_4·0.625Et_2O suitable for X-ray analysis were obtained by protonation with HBF_4·Et_2O and subsequent recrystallization from methanol/diethyl ether (1.5 mL/15 mL). ^{1}H NMR (δ, CD_3OD): 0.80 (d, $^3J_{HH}$ = 6.7 Hz, 3H, CH_3), 1.59 (d, $^3J_{HH}$ = 6.4 Hz, 3H, CH_3), 3.06, 3.50 (m, 1H each, $CHCH_3$), 3.91, 4.42 (d, $^3J_{HH}$ = 13.1 Hz, 1H each, NCH_2CPh_2), 4.58, 4.76 (d, $^3J_{HH}$ = 13.1 Hz, 1H each, NCH_2Ph), 6.88 (m, 2H, C_6H_5), 7.29 (m, 5H, C_6H_5), 7.34 (m, 1H, C_6H_5), 7.42 (m, 2H, C_6H_5), 7.58 (m, 3H, C_6H_5), 7.67 (m, 2H, C_6H_5). The thoroughly dried sample was found to lose the solvating molecule, on the basis of ^{1}H NMR spectroscopy and combustion analysis. Anal. Calcd for $C_{25}H_{28}BF_4N$: C, 69.94; H, 6.57; N, 3.26. Found: C, 70.06; H, 6.44; N, 3.18.

*N-Benzyl-3-methyl-2-azaspiro[4.5]decan-4-ol (****4n****).* ^{1}H NMR (δ, $CDCl_3$): 1.20–1.60 (m, 10H, $(CH_2)_5$), 1.25 (d, $^3J_{HH}$ = 5.8 Hz, 3H, CH_3), 2.04, 2.83 (d, $^2J_{HH}$ = 9.6 Hz, 1H each, NCH_2), 2.31 (m, 1H, CH_3CH), 3.16, 4.00 (d, $^2J_{HH}$ = 13.4 Hz, 1H each, $PhCH_2$), 3.33 (d, $^3J_{HH}$ = 6.7 Hz, 1H, CHOH), 7.21–7.31 (m, 5H, C_6H_5). ^{13}C{^{1}H} NMR (δ, $CDCl_3$): 17.5, 22.9, 23.5, 26.1, 31.3, 36.7, 42.1, 57.6, 62.7, 66.3, 86.0, 126.7, 128.1, 128.6, 139.4. HRMS (ESI-TOF): m/z calcd for $C_{17}H_{25}NO + H^+$ 260.2009, found 260.2008.

Computational Studies. All calculations were performed by means of the density functional theory in the Gaussian 09 program[43] using an exchange-correlation hybrid functional, denoted as MPW1PW91. For this density functional method, the correlation functional is from Perdew–Wang 1991 (PW91),[44] while the exchange functional is from Barone's modified PW91 (MPW1).[45] Geometry optimizations were performed using SDD effective core potential (ECP)[46] along with its associated basis set for iridium and 6-31G(d,p) basis set[47] for the other typical atoms. This combination of the functional and the basis sets reproduced the structure of the ethylene complex **8** confirmed by X-ray analysis. Thermochemical values for each optimized structure were obtained for 298.15 K and 1.0 atm by frequency analyses using the same basis sets and ECP within the harmonic approximation.

Representative Procedures for Kinetic Experiments. A solution of **8** in C_6D_6 was prepared and , stored under an argon atmosphere at 0 °C, and a requisite amount of the solution was taken for each experiment. To an NMR tube equipped with a J. Young valve was added **3d** (39.6 mg, 121 μmol), 1,3,5-trimethoxybenzene (as an internal standard, 11.2 mg, 66.6 μmol), and the C_6D_6 solution of **8** (12.0 mM, 0.50 mL, 6.0 μmol). The time course of the reaction was monitored by the VT-NMR spectrum, and the concentration of the substrate was calculated by comparing the peak intensity of the vinylic protons at the 5-position to that of the methoxy protons of the internal standard. The moment at which the probe temperature of the NMR spectrometer reached the intended temperature was set as t = 0 s. For the investigation of the effect of catalyst concentration, less than 0.5 mL of the catalyst solution was taken, and the mixture was diluted with additional C_6D_6 to the intended concentration.

■ ASSOCIATED CONTENT

Ⓢ Supporting Information

Tables, figures, and CIF files giving X-ray crystallographic data for **4f**·HBF_4·0.625Et_2O, **8**·Et_2O, **9a**·0.5H_2O, **9b**·0.5H_2O, **10**, and **11a** and details of the NOE experiments, the computational studies, and the kinetic experiments. This material is available free of charge via the Internet at http://pubs.acs.org.

AUTHOR INFORMATION

Corresponding Author

*E-mail: skuwata@apc.titech.ac.jp (S.K.); tikariya@apc.titech.ac.jp (T.I.).

Notes

The authors declare no competing financial interest.

ACKNOWLEDGMENTS

This work was supported by a Grant-in-Aid for Scientific Research (S) (22225004) from the Ministry of Education, Culture, Sports, Science and Technology of Japan. Y.K. acknowledges a Japan Society for the Promotion of Science Research Fellowship for Young Scientists.

REFERENCES

(1) (a) Müller, T. E.; Beller, M. *Chem. Rev.* **1998**, *98*, 675. (b) Müller, T. E.; Hultzsch, K. C.; Yus, M.; Foubelo, F.; Tada, M. *Chem. Rev.* **2008**, *108*, 3795. (c) Chemler, S. R. *Org. Biomol. Chem.* **2009**, *7*, 3009. (d) Hartwig, J. F. *Organotransition Metal Chemistry. From Bonding to Catalysis*; University Science Books: Sausalito, CA, 2010; pp 700−717. (e) Yadav, J. S.; Antony, A.; Srinivasa Rao, T.; Subba Reddy, B. V. *J. Organomet. Chem.* **2011**, *696*, 16.

(2) (a) Hong, S.; Marks, T. J. *Acc. Chem. Res.* **2004**, *37*, 673. (b) Zi, G. *J. Organomet. Chem.* **2011**, *696*, 68. (c) Hannedouche, J.; Collin, J.; Trifonov, A.; Schulz, E. *J. Organomet. Chem.* **2011**, *696*, 255. (d) Zhang, Y.; Yao, W.; Li, H.; Mu, Y. *Organometallics* **2012**, *31*, 4670. (e) Otero, A.; Lara-Sánchez, A.; Nájera, C.; Fernández-Baeza, J.; Márquez-Segovia, I.; Castro-Osma, J. A.; Martínez, J.; Sánchez-Barba, L. F.; Rodríguez, A. M. *Organometallics* **2012**, *31*, 2244. (f) Zhang, X.; Emge, T. J.; Hultzsch, K. C. *Angew. Chem., Int. Ed.* **2012**, *51*, 394. (g) Chapurina, Y.; Ibrahim, H.; Guillot, R.; Kolodziej, E.; Collin, J.; Trifonov, A.; Schulz, E.; Hannedouche, J. *J. Org. Chem.* **2011**, *76*, 10163. (h) Wang, X.; Chen, Z.; Sun, X.-L.; Tang, Y.; Xie, Z. *Org. Lett.* **2011**, *13*, 4758. (i) Wixey, J. S.; Ward, B. D. *Chem. Commun.* **2011**, *47*, 5449. (j) Benndorf, P.; Jenter, J.; Zielke, L.; Roesky, P. W. *Chem. Commun.* **2011**, *47*, 2574. (k) Vitanova, D. V.; Hampel, F.; Hultzsch, K. C. *J. Organomet. Chem.* **2011**, *696*, 321. (l) Hangaly, N. K.; Petrov, A. R.; Rufanov, K. A.; Harm, K.; Elfferding, M.; Sundermeyer, J. *Organometallics* **2011**, *30*, 4544. (m) Queffelec, C.; Boeda, F.; Pouilhès, A.; Meddour, A.; Kouklovsky, C.; Hannedouche, J.; Collin, J.; Schulz, E. *ChemCatChem* **2011**, *3*, 122. (n) Arrowsmith, M.; Crimmin, M. R.; Barrett, A. G. M.; Hill, M. S.; Kociok-Köhn, G.; Procopiou, P. A. *Organometallics* **2011**, *30*, 1493.

(3) (a) Leitch, D. C.; Platel, R. H.; Schafer, L. L. *J. Am. Chem. Soc.* **2011**, *133*, 15453. (b) Manna, K.; Xu, S.; Sadow, A. D. *Angew. Chem., Int. Ed.* **2011**, *50*, 1865.

(4) (a) Dorta, R. In *Iridium Complexes in Organic Synthesis*; Oro, L. A., Claver, C., Eds.; Wiley-VCH: Weinheim, Germany, 2009; pp 145−172. (b) Hesp, K. D.; Stradiotto, M. *ChemCatChem* **2010**, *2*, 1192.

(5) Julian, L. D.; Hartwig, J. F. *J. Am. Chem. Soc.* **2010**, *132*, 13813.

(6) Liu, Z.; Hartwig, J. F. *J. Am. Chem. Soc.* **2008**, *130*, 1570.

(7) (a) Bender, F.; Hudson, W. B.; Widenhoefer, R. A. *Organometallics* **2008**, *27*, 2356. (b) Pissarek, J.-W.; Schlesiger, D.; Roesky, P. W.; Blecherta, S. *Adv. Synth. Catal.* **2009**, *351*, 2081.

(8) (a) Bauer, E. B.; Andavan, G. T. S.; Hollis, T. K.; Rubio, R. J.; Cho, J.; Kuchenbeiser, G. R.; Helgert, T. R.; Letko, C. S.; Tham, F. S. *Org. Lett.* **2008**, *10*, 1175. (b) Bender, C. F.; Widenhoefer, R. A. *J. Am. Chem. Soc.* **2005**, *127*, 1070.

(9) Hesp, K. D.; Tobisch, S.; Stradiotto, M. *J. Am. Chem. Soc.* **2010**, *132*, 413.

(10) Liu, Z.; Yamamichi, H.; Madrahimov, S. T.; Hartwig, J. F. *J. Am. Chem. Soc.* **2011**, *133*, 2772.

(11) (a) Hua, C.; Vuong, K. Q.; Bhadbhade, M.; Messerle, B. A. *Organometallics* **2012**, *31*, 1790. (b) Specht, Z. G.; Cortes-Llamas, S. A.; Tran, H. N.; van Niekerk, C. J.; Rancudo, K. T.; Golen, J. A.; Moore, C. E.; Rheingold, A. L.; Dwyer, T. J.; Grotjahn, D. B. *Chem. Eur. J.* **2011**, *17*, 6606. (c) Hesp, K. D.; McDonald, R.; Stradiotto, M. *Can. J. Chem.* **2010**, *88*, 700. (d) Lavery, C. B.; Ferguson, M. J.; Stradiotto, M. *Organometallics* **2010**, *29*, 6125. (e) Kitahara, H.; Sakurai, H. *Chem. Lett.* **2010**, *39*, 46. (f) Ohmiya, H.; Moriya, T.; Sawamura, M. *Org. Lett.* **2009**, *11*, 2145.

(12) Jung, M. E.; Piizzi, G. *Chem. Rev.* **2005**, *105*, 1735.

(13) Shen, X.; Buchwald, S. L. *Angew. Chem., Int. Ed.* **2010**, *49*, 564.

(14) (a) Ikariya, T. *Bull. Chem. Soc. Jpn.* **2011**, *84*, 1. (b) Ikariya, T.; Kuwata, S.; Kayaki, Y. *Pure Appl. Chem.* **2010**, *82*, 1471. (c) Dub, P. A.; Wang, H.; Watanabe, M.; Gridnev, I. D.; Ikariya, T. *Tetrahedron Lett.* **2012**, *53*, 3452. (d) Sato, Y.; Kayaki, Y.; Ikariya, T. *Chem. Commun.* **2012**, *48*, 3635. (e) Hasegawa, Y.; Gridnev, I. D.; Ikariya, T. *Bull. Chem. Soc. Jpn.* **2012**, *85*, 316. (f) Watanabe, M.; Kashiwame, Y.; Kuwata, S.; Ikariya, T. *Eur. J. Inorg. Chem.* **2012**, 504. (g) Touge, T.; Hakamata, T.; Nara, H.; Kobayashi, T.; Sayo, N.; Saito, T.; Kayaki, Y.; Ikariya, T. *J. Am. Chem. Soc.* **2011**, *133*, 14960. (h) Ito, M.; Ootsuka, T.; Watari, R.; Shiibashi, A.; Himizu, A.; Ikariya, T. *J. Am. Chem. Soc.* **2011**, *133*, 4240. (i) Ito, M.; Shiibashi, A.; Ikariya, T. *Chem. Commun.* **2011**, *47*, 2134.

(15) (a) Kuwata, S.; Ikariya, T. *Chem. Eur. J.* **2011**, *17*, 3542. (b) Kashiwame, Y.; Watanabe, M.; Araki, K.; Kuwata, S.; Ikariya, T. *Bull. Chem. Soc. Jpn.* **2011**, *84*, 251. (c) Yoshinari, A.; Tazawa, A.; Kuwata, S.; Ikariya, T. *Chem. Asian J.* **2012**, *7*, 1417.

(16) (a) Praneeth, V. K. K.; Ringenberg, M. R.; Ward, T. R. *Angew. Chem., Int. Ed.* **2012**, *51*, 10228. (b) van der Vlugt, J. I. *Eur. J. Inorg. Chem.* **2012**, 363. (c) Schneider, S.; Meiners, J.; Askevold, B. *Eur. J. Inorg. Chem.* **2012**, 412. (d) Askevold, B.; Roesky, H. W.; Schneider, S. *ChemCatChem* **2012**, *4*, 307. (e) Gunanathan, C.; Milstein, D. *Acc. Chem. Res.* **2011**, *44*, 588. (f) DuBois, D. L.; Bullock, R. M. *Eur. J. Inorg. Chem.* **2011**, 1017. (g) Crabtree, R. H. *New J. Chem.* **2011**, *35*, 18. (h) Meeuwissen, J.; Reek, J. N. H. *Nat. Chem* **2010**, *2*, 615. (i) Grotjahn, D. B. *Chem. Lett.* **2010**, *39*, 908. (j) Morris, R. H. *Chem. Soc. Rev.* **2009**, *38*, 2282. (k) Grützmacher, H. *Angew. Chem., Int. Ed.* **2008**, *47*, 1814.

(17) Kashiwame, Y.; Kuwata, S.; Ikariya, T. *Chem. Eur. J.* **2010**, *16*, 766.

(18) Davis and co-workers independently synthesized **6** and determined the crystal structure: Boutadla, Y.; Davis, D. L.; Jones, R. C.; Singh, K. *Chem. Eur. J.* **2011**, *17*, 3438.

(19) Arita, S.; Koike, T.; Kayaki, Y.; Ikariya, T. *Organometallics* **2008**, *27*, 2795.

(20) Examples of catalytic intramolecular hydroamination affording products with two adjacent stereocenters: (a) Kim, Y. K.; Livinghouse, T. *Angew. Chem., Int. Ed.* **2002**, *41*, 3645. (b) Hoover, J. M.; DiPasquale, A.; Mayer, J. M.; Michael, F. E. *J. Am. Chem. Soc.* **2010**, *132*, 5043. (c) Zhang, Z.; Liu, C.; Kinder, R. E.; Han, X.; Qian, H.; Widenhoefer, R. A. *J. Am. Chem. Soc.* **2006**, *128*, 9066. (d) Zhang, W.; Werness, J. B.; Tang, W. *Org. Lett.* **2008**, *18*, 7248.

(21) We replicated Hartwig's protocol[6] and subjected the major product to the NOE experiments. The obtained difference spectrum did not indicate an NOE correlation between the methyl protons and the vicinal methine proton, while a correlation between the two vicinal methine protons was observed, suggesting that the major product therein is the *cis* isomer against the original assignment (see the Supporting Information).[6]

(22) McDonald, R. I.; Liu, G.; Stahl, S. S. *Chem. Rev.* **2011**, *111*, 2981.

(23) Liu, C.; Bender, C. F.; Han, X.; Widenhoefer, R. A. *Chem. Commun.* **2007**, 3607.

(24) Tobisch, S. *Chem. Eur. J.* **2012**, *18*, 7248.

(25) Hartwig, J. F. *Organotransition Metal Chemistry. From Bonding to Catalysis*; University Science Books: Sausalito, CA, 2010; pp 427−435.

(26) Muñiz, K.; Lishchynskyi, A.; Streuff, J.; Nieger, M.; Escudero-Adán, E. C.; Belmonte, M. M. *Chem. Commun.* **2011**, *47*, 4911.

(27) (a) Díez, J.; Gamasa, M. P.; Gimeno, J.; Paredes, P. *Organometallics* **2005**, *24*, 1799. (b) Gutiérrez-Puebla, E.; Monge, Á.; Nicasio, M. C.; Pérez, P. J.; Poveda, M. L.; Rey, L.; Ruíz, C.; Carmona, E. *Inorg. Chem.* **1998**, *37*, 4538. (c) Sola, E.; Navarro, J.; López, J. A.; Lahoz, F. J.; Oro, L. A.; Werner, H. *Organometallics* **1999**, *18*, 3534.

(28) Gordon, A. J.; Ford, R. A. *The Chemist's Companion: A Handbook of Practical Data, Techniques, and References*; Wiley-Interscience: Hoboken, NJ, 1972; p 108.
(29) (a) Murata, K.; Konishi, H.; Ito, M.; Ikariya, T. *Organometallics* **2002**, *21*, 253. (b) Watanabe, M.; Murata, K.; Ikariya, T. *J. Am. Chem. Soc.* **2003**, *125*, 7508. (c) Fulton, J. R.; Holland, A. W.; Fox, D. J.; Bergman, R. G. *Acc. Chem. Res.* **2002**, *35*, 44. (d) Gunnoe, T. B. *Eur. J. Inorg. Chem.* **2007**, 1185.
(30) Koike, T.; Ikariya, T. *J. Organomet. Chem.* **2007**, *692*, 408.
(31) Julian and Hartwig proposed that lone pair electrons in the aminophosphine ligand of their rhodium catalyst may promote the protonolysis of the metal−carbon bond.[5]
(32) Crumpton-Bregel, D. M.; Goldberg, K. I. *J. Am. Chem. Soc.* **2003**, *125*, 9442 and references therein.
(33) McKinney Brooner, R. E.; Widenhoefer, R. A. *Chem. Eur. J.* **2011**, *17*, 6170.
(34) (a) Minatti, A.; Muñiz, K. *Chem. Soc. Rev.* **2007**, *36*, 1142. (b) Kotov, V.; Scarborough, C. C.; Stahl, S. S. *Inorg. Chem.* **2007**, *46*, 1910.
(35) A different type of bifunctional mechanism featuring proton transfer from a ligated protic amine to the uncoordinated olefin bond through a six-membered transition state has recently been proposed for alkaline-earth-metal and zirconium catalysts: Liu, B.; Roisnel, T.; Carpentier, J.-F.; Sarazin, Y. *Angew. Chem., Int. Ed.* **2012**, *51*, 4943. See also ref 3.
(36) Hong, S.; Tian, S.; Metz, M. V.; Marks, T. J. *J. Am. Chem. Soc.* **2003**, *125*, 14768.
(37) Stang, E. M.; White, M. C. *J. Am. Chem. Soc.* **2011**, *133*, 14892.
(38) Acemoglu, L.; Williams, J. M. J. *Adv. Synth. Catal.* **2001**, *343*, 75.
(39) Dent, W. T.; Long, R.; Wilkinson, A. J. *J. Chem. Soc.* **1964**, 1585.
(40) Kondo, T.; Okada, T.; Mitsudo, T. *J. Am. Chem. Soc.* **2002**, *124*, 186.
(41) *CrystalStructure 4.0: Crystal Structure Analysis Package*, Rigaku Corp., Tokyo 196-8666, Japan, 2000−2010
(42) SIR92: Altomare, A.; Cascarano, G.; Giacovazzo, C.; Guagliardi, A.; Burla, M.; Polidori, G.; Camalli, M. *J. Appl. Crystallogr.* **1994**, *27*, 435.
(43) Frisch, M. J.; Trucks, G. W.; Schlegel, H. B.; Scuseria, G. E.; Robb, M. A.; Cheeseman, J. R.; Scalmani, G.; Barone, V.; Mennucci, B.; Petersson, G. A.; Nakatsuji, H.; Caricato, M.; Li, X.; Hratchian, H. P.; Izmaylov, A. F.; Bloino, J.; Zheng, G.; Sonnenberg, J. L.; Hada, M.; Ehara, M.; Toyota, K.; Fukuda, R.; Hasegawa, J.; Ishida, M.; Nakajima, T.; Honda, Y.; Kitao, O.; Nakai, H.; Vreven, T.; Montgomery, J. A., Jr.; Peralta, J. E.; Ogliaro, F.; Bearpark, M.; Heyd, J. J.; Brothers, E.; Kudin, K. N.; Staroverov, V. N.; Kobayashi, R.; Normand, J.; Raghavachari, K.; Rendell, A.; Burant, J. C.; Iyengar, S. S.; Tomasi, J.; Cossi, M.; Rega, N.; Millam, J. M.; Klene, M.; Knox, J. E.; Cross, J. B.; Bakken, V.; Adamo, C.; Jaramillo, J.; Gomperts, R.; Stratmann, R. E.; Yazyev, O.; Austin, A. J.; Cammi, R.; Pomelli, C.; Ochterski, J. W.; Martin, R. L.; Morokuma, K.; Zakrzewski, V. G.; Voth, G. A.; Salvador, P.; Dannenberg, J. J.; Dapprich, S.; Daniels, A. D.; Farkas, Ö.; Foresman, J. B.; Ortiz, J. V.; Cioslowski, J.; Fox, D. J. *Gaussian 09, Revision B.01*; Gaussian, Inc., Wallingford, CT, 2009.
(44) Perdew, J. P.; Wang, Y. In *Electronic Structures of Solids 91*; Ziesche, P., Eschrig, H., Eds.; Akademie-Verlag: Berlin, 1991.
(45) Adamo, C.; Barone, V. *J. Chem. Phys.* **1998**, *108*, 664.
(46) (a) Dunning, T. H., Jr.; Hay, P. J. In *Modern Theoretical Chemistry*; Schaefer, H. F., III, Ed.; Plenum: New York, 1976; Vol. 3, p 1. (b) Leininger, T; Nicklass, A.; Stoll, H.; Dolg, M.; Schwerdtfeger, P. *J. Chem. Phys.* **1996**, *105*, 1052.
(47) Raghavachari, K.; Binkley, J. S.; Seeger, R.; Pople, J. A. *J. Chem. Phys.* **1980**, *72*, 650.

■ NOTE ADDED AFTER ASAP PUBLICATION

In the version of this paper published on November 19, 2012, a statement near the end of the paper regarding the mechanism was incorrect. The version that appears as of December 10, 2012, is correct.